An impedance model for Analysis of EIS of Polymer Electrolyte Fuel Cells under Platinum Oxidation and Hydrogen Peroxide Formation in the Cathode.

Samuel Cruz-Manzo[1*], Ulises Perezmitre-Cruz[1], Paul Greenwood[2], and Rui Chen[2]

[1]Abastecedora Electrica Tehuacan, Engineering Division, Tehuacan, Puebla, 75700, Mexico

[2]Department of Aeronautical and Automotive Engineering, Loughborough University, Leicestershire LE11 3TU, United Kingdom

*E-mail: s.cruz-manzo@hotmail.com

Abstract

In this study, an impedance model based on electrochemical theory of platinum oxide formation has been developed and combined with the impedance model based on hydrogen peroxide formation during the oxygen reduction reaction (ORR) and reported in a previous study to charaterise inductive loops in impedance spectra of polymer electrolyte fuel cells (PEFCs). To validate the theoretical treatment, the simulated frequency response predicted by the theoretical model is compared against electrochemical impedance spectroscopy (EIS) measurements carried out in an open-cathode 16 cm^2 H_2/air PEFC stack at three different current densities. The results show that neither model in isolation (hydrogen peroxide nor platinum oxide models) can accurately reproduce the inductive loops in the EIS measurements at low frequencies. By deriving a model considering kinetics of hydrogen peroxide and platinum oxide formation, it is possible to reproduce the inductive loops at low frequencies and to estimate the DC polarisation resistance related to the slope of the polarisation curve as frequency reaches zero during EIS. This study demonstrates that different mechanisms that cause PEFC degradation and low performance could be manifested in EIS measurements simultaneously. The resulting model could support other electrochemical techniques to quantify the rates of hydrogen peroxide and platinum oxide formation during the ORR that limit the performance of PEFCs.

1. Introduction

Polymer electrolyte fuel cells (PEFCs) are considered a future source of propulsion for stationary and mobile applications. Material degradation is one of the concerns hindering the delivery and commercialisation of PEFCs as a reliable source of energy. PEFCs for automotive applications are exposed to harsh operational conditions which can lead to a loss of the active area in the electrodes [1]. Electrochemical impedance

spectroscopy (EIS) is a powerful technique that can be applied in-situ to de-convolute the various loss mechanisms in the PEFC that occur at different rates. The frequency response of a PEFC that results from EIS is in essence characterised by energy dissipating and energy storing elements of the cell. Although the use of equivalent circuits is often an adequate approach, some electrochemical processes are not adequately described by electrical components. In which case, it is necessary to adopt a more rigorous approach of describing processes through the use of differential equations to describe the physics of the electrochemical system at the frequency domain. As reported by Macdonald [2] electrical circuits are analogs and not models, therefore the information that they deliver related to the physical processes occurring within the PEFC is limited. The interpretation of electrochemical mechanisms which are truly occurring in the PEFC using EIS will only be possible through mathematical models or electrical circuits derived from fundamental electrochemical theory [3].

EIS measurements with positive imaginary components at low frequencies are known as an inductive loop. It has been demonstrated that inductive loops are related to electrochemical processes and are consistent with Kramer-Kronig relations [4]. Studies in the literature have related the inductive loop to side and intermediate reactions involved during the oxygen reduction reaction (ORR). EIS models have been reported in the literature to relate the inductive loops with electrochemical mechanisms which could cause degradation and low performance during PEFC operation. Roy *et al.* [4] developed impedance models of PEFCs based on the intermediate species such as rate of oxidation and dissolution of platinum and hydrogen peroxide formation during the ORR. The models predicted that the mechanisms of platinum oxidation and hydrogen peroxide can be attributed to an inductive loop at low frequencies. An impedance model which demonstrates that slow Pt oxide kinetics during the ORR are related to inductive loops in EIS measurements of PEFCs has been reported by Mathias *et. al.* [5]. A recent impedance model developed by Setzler and Fuller [6] demonstrated that the growth of an oxide layer during the ORR is shown to produce a low frequency inductive loop. The impedance models reported in the literature have been focused on the study of a single electrochemical process (e.g. platinum oxide formation) and not considering combined electrochemical processes (e.g. platinum oxide formation and hydrogen peroxide formation) that can lead to inductive loops at low frequencies. In a previous study [7], an impedance model that predicts hydrogen peroxide formation during the ORR was developed and validated with EIS measurements featuring inductive loops and reported in an earlier study [8]. The EIS measurements previously reported allowed the validation of an electrical circuit which relates adsorbed intermediate species during the ORR with inductive loops [8]. However the previous electrical circuit [8] did not

define what adsorbed intermediate species were present during PEFC operation. In this study, firstly an impedance model considering only kinetics of platinum oxide formation is developed and validated with the EIS measurements previously reported [7,8]. The reason for validating the impedance model based on platinum oxidation with the EIS measurements reported in the previous study [7,8] is due to the slight difference in the shape of the inductive loop from experimental data compared to the simulated data from the model predicting hydrogen peroxide formation [7]. This difference reveals that not only hydrogen peroxide formation is present in the EIS measurements but also platinum oxide formation that can cause fuel cell degradation. Based on the validation of the platinum oxide impedance model, an impedance model which combines hydrogen peroxide formation with platinum oxide formation is developed and validated with EIS measurements. This impedance model with EIS could support other electrochemical techniques as reported by Roy *et al.* [9] to study mechanisms that cause degradation and low performance in PEFCs.

2. Electrochemical mechanisms of platinum oxide formation

The formation of platinum oxide (PtO) reaction has been reported in the literature [10] as:

$$Pt + H_2O \underset{kb}{\overset{kf}{\leftrightarrow}} PtO + 2H^+ + 2e^- \tag{1}$$

Reaction (1) can be separated into a two-step process through only one electron transfer [11]. The first step involves the formation of Pt-OH and secondly Pt-OH is oxidized to Pt-O [11]. Adsorption of Pt-OH and Pt-O on Pt electrodes has been investigated through X-ray absorption spectroscopy and X-ray photoelectron spectroscopy [12,13]. The role of Pt-OH on the ORR was studied by Liu *et al.* [14] assuming that Pt-OH is the simplest Pt oxide acting as an intermediate or poison during the ORR. For simplicity, in this study it is considered that Pt-O is the Pt oxide absorbed onto free Pt which affects the kinetics of the ORR.

The forward and backward current densities corresponding to reaction (1) have been reported in the literature [10] as:

$$i_{Pt,f} = nFk_{Pt,f}\lambda c_{H_2O}(1-\gamma_{PtO})\exp\left(b_{Pt,f}V\right) \tag{2}$$

$$i_{Pt,b} = nFk_{Pt,b}c_{H^+}^2\gamma_{PtO}\exp\left(-b_{Pt,b}V\right) \tag{3}$$

where F is the Faraday constant, $k_{Pt,f}$ and $k_{Pt,b}$ are the forward and backward rate constants which depend on the global order of reaction, λ is the moles of adsorption sites per unit of platinum area, c_i is the concentration

at the electrode surface for species *i*, *n* is the number of electrons transferred during the reaction, γ_{PtO} is the fractional surface coverage of platinum oxide, b_i is the inverse Tafel slope, and *V* is the electrode potential.

The following assumptions are considered to facilitate the mathematical treatment:

The rate of platinum oxidation represented through reaction (1) is a function of the concentration of the chemical species, $c_{H^+}^2$ and c_{H_2O}. The effect of water and oxygen concentrations on platinum oxidation has been studied by Xu *et al.* [11], where the rate of platinum oxidation increases with oxygen and water concentrations; nevertheless, Liu *et al*. [14] reported that oxygen concentration does not contribute to the formation of platinum oxide. The concentration of the species for reaction (1) is considered at equilibrium conditions c_{eq,H^+}^2, c_{eq,H_2O}; no concentration gradient effect of protons and water on the rate of platinum oxide formation. When increasing current during PEFC operation the concentration of protons yields to an increase in water concentration in the cathode catalyst layer (CCL); therefore in this study the concentration gradient of protons and water on platinum oxidation is neglected. Yadav *et al.* [15] demonstrated that increasing the concentration of sulphuric acid, which increases proton concentration, enhances the rate of platinum oxidation. Darling and Meyers [16] developed a model that describes the kinetics of platinum oxidation in PEFCs. The model considers the rate of change with respect to time of platinum particle radius, concentration of ionic platinum species, and fraction of platinum surface covered by PtO. A model that describes the physical theory of platinum nanoparticle dissolution in PEFCs is presented by Rinaldo *et al.* [17]. The model incorporates the particle radius distribution, and considers kinetic mechanisms of platinum dissolution, platinum oxide formation, and platinum oxide dissolution. A complete impedance model for platinum oxidation in PEFCs should include the kinetic expressions, such as the rate of change with respect to platinum particle radius, concentration of ionic platinum species, and fraction of platinum surface covered by PtO, reported by Darling and Meyers [16] and Rinaldo *et al.* [17]. Nevertheless this mathematical treatment could result in an analytical expression rather than an electrical circuit for analysis of PEFCs under platinum oxidation using EIS. In addition this would make it difficult to be applied in real world EIS measurements and using commercial software (e.g. ZView Scribner Associates Inc.) which commonly utilizes electrical circuits for EIS analysis. Also an increase in the number of parameters in an equation that represents the PEFC impedance response may lead to increased error in the resulting fitted values with experimental EIS. The current study simplifies the mathematical treatment by neglecting the change of platinum particle radius with respect to time which has an effect on particle-size distribution in the CCL. This

simplification will allow the model to be represented as an electrical circuit for application with real world EIS measurements and using commercial software.

Taking into account the assumptions previously mentioned, Eqs. 2 and 3 can be defined as:

$$i_{Pt,f} = nFk_{Pt,f}\lambda c_{eq,H_2O}(1-\gamma_{PtO})\exp(b_{Pt,f}V) \tag{4}$$

$$i_{Pt,b} = nFk_{Pt,b}c_{eq,H^+}^2\gamma_{PtO}\exp(-b_{Pt,b}V) \tag{5}$$

where, $c_{eq,i}$ represents the concentration at equilibrium conditions as it is assumed that surface concentration of water and protons through the CCL is constant.

Under equilibrium conditions, the reaction (1) proceeds in both directions simultaneously at the same rate. Therefore the potential at equilibrium is equal to the potential of the electrode, $V_{eq} = V$. In addition, the concentration (denominated as bulk concentration under this state) are the same for the chemical species, $c_{eq,i}$. The rate at which the forward and backward transfer of charge occurs at equilibrium is known as the exchange current, i_0. As such:

$$i_{0_{Pt}} = nFk_{Pt,f}\lambda c_{eq,H_2O}(1-\gamma_{eq,PtO})\exp(b_{Pt,f}V_{eq,Pt,f}) = nFk_{Pt,b}c_{eq,H^+}^2\gamma_{eq,PtO}\exp(-b_{Pt,b}V_{eq,Pt,b}) \tag{6}$$

where $\gamma_{eq,PtO}$ is the fractional surface coverage of platinum oxide under equilibrium conditions and $V_{eq,i}$ is the equilibrium potential.

Dividing both terms of Eq. 4 by $(1-\gamma_{eq,PtO})\exp(b_{Pt,f}V_{eq,Pt,f})$ and similarly Eq. 5 by $\gamma_{eq,PtO}\exp(-b_{Pt,b}V_{eq,Pt,b})$, and substituting Eq. 6 yields:

$$i_{Pt,f} = i_{0,Pt}\frac{(1-\gamma_{PtO})}{(1-\gamma_{eq,PtO})}\exp(b_{Pt,f}(V-V_{eq,Pt,f})) \tag{7}$$

$$i_{Pt,b} = i_{0,Pt}\frac{\gamma_{PtO}}{\gamma_{eq,PtO}}\exp(-b_{Pt,b}(V-V_{eq,Pt,b})) \tag{8}$$

The total current density for reaction (1) is expressed as the difference between the forward current Eq. 7 and the backward current Eq. 8, $i_{Pt} = i_{Pt,f} - i_{Pt,b}$:

$$i_{Pt} = i_{0,Pt}\frac{(1-\gamma_{PtO})}{(1-\gamma_{eq,PtO})}\exp(b_{Pt,f}(V-V_{eq,Pt,f})) - i_{0,Pt}\frac{\gamma_{PtO}}{\gamma_{eq,PtO}}\exp(-b_{Pt,b}(V-V_{eq,Pt,b})) \tag{9}$$

The change of platinum particle radius with respect to time which has an effect on particle-size distribution in

the CCL is neglected in this study. Platinum oxide formation with respect to time is considered. Assuming that the formation of platinum oxide is governed by the Langmuir isothermal, it is possible to define the variation rate of γ_{PtO} as [18]:

$$nF\lambda \frac{d\gamma_{PtO}}{dt} = i_{Pt} \tag{10}$$

Substituting Eq. 9 into Eq. 10 yields:

$$nF\lambda \frac{d\gamma_{PtO}}{dt} = i_{0,Pt} \frac{(1-\gamma_{PtO})}{(1-\gamma_{eq,PtO})} \exp\left(b_{Pt,f}\left(V - V_{eq,Pt,f}\right)\right) - i_{0,Pt} \frac{\gamma_{PtO}}{\gamma_{eq,PtO}} \exp\left(-b_{Pt,b}\left(V - V_{eq,Pt,b}\right)\right) \tag{11}$$

2.1 Platinum oxidation during oxygen reduction reaction

The ORR can be considered as simple reaction kinetics:

$$O_2 + 4H^+ + 4e^- \rightarrow 2H_2O \tag{12}$$

The current that represents the ORR at the cathode is expressed as [10]:

$$i_{O_2} = -nFk_{O_2} c_{O_2} c_{eq,H^+}^{3/2} \exp\left(-b_{O2} V\right) \tag{13}$$

where k_{O_2} is the rate constant which depends on the global order of reaction, c_{O_2} is the concentration of oxygen at the electrode surface, and $c_{eq,H^+}^{3/2}$ is the equilibrium (bulk) concentration of protons where in this study it is considered that the concentration of protons from the CCL-PEM interface to the Pt-C agglomerates is constant.

The rate constant during the ORR can be related to the rate of platinum oxide formation by considering an effective rate constant that relates the rate constant on a platinum site as such:

$$k_{O_2} = k_{Pt}\left(1 - \gamma_{PtO}\right) \tag{14}$$

Substituting Eq. 14 into Eq. 13 yields:

$$i_{O_2} = -nFk_{Pt}\left(1 - \gamma_{PtO}\right) c_{O_2} c_{eq,H^+}^{3/2} \exp\left(-b_{O2} V\right) \tag{15}$$

Eq. 15 demonstrates that if the fractional surface coverage of platinum oxide γ_{PtO} increases, the PEFC current becomes lower.

The exchange current density for ORR (Eq. 12) at equilibrium conditions with $V = V_{eq,o_2}$ and considering the fractional surface coverage of platinum oxide can be defined as:

$$i_{0,O_2} = nFk_{Pt}\left(1-\gamma_{eq,PtO}\right)c_{eq,O_2}c_{eq,H^+}^{3/2}\exp\left(-b_{O2}V_{eq,o_2}\right) \tag{16}$$

where i_{0,O_2} represents the exchange current density, $\gamma_{eq,PtO}$ is the fractional surface coverage of platinum oxide under equilibrium conditions and V_{eq,O_2} is the equilibrium potential.

Multypling Eq. 15 by $c_{eq,O_2}\left(1-\gamma_{eq,H_2O_2}\right)\exp\left(-b_{O_2}V_{eq,O_2}\right)$ and substituting Eq. 16 yields:

$$i_{O_2} = -i_{0,O_2}\frac{c_{O_2}}{c_{eq,O_2}}\frac{\left(1-\gamma_{PtO}\right)}{\left(1-\gamma_{eq,PtO}\right)}\exp\left[-b_{O_2}\left(V-V_{eq,O_2}\right)\right] \tag{17}$$

2.2 ac impedance response

If a small ac perturbation is applied to the working electrode, the EIS technique allows the use of a linear equation to simulate impedance spectra. A linear model can be derived using the Taylor series expansion as expressed below:

$$\tilde{i} = \left(\frac{\partial i_{O_2}}{\partial V}\right)_{ss}\tilde{V} + \left(\frac{\partial i_{O_2}}{\partial \gamma_{PtO}}\right)_{ss}\tilde{\gamma}_{PtO} \tag{18}$$

To facilitate the mathematical treatment, the small disturbance of oxygen from the ac perturbation is not considered in Eq. 18 at first. One of the advantages of the EIS technique relies on the fact that it is possible to decouple physical processes with different time constant and different frequency dependence. No coupling between mass transport and surface coverage can exist during EIS measurements. A priori decoupling between oxygen transport limitations and platinum oxide coverage is considered in Eq. 18 in which the perturbation of the oxygen concentration in the CCL is neglected at first. Thereafter the Warburg impedance, which has been broadly used in the analysis of oxygen transport limitations in experimental EIS measurements, will be incorporated in the mathematical treatment to account for small disturbance of oxygen from the ac perturbation. Based on experimental EIS measurements in which physical parameters are measured across the entire CCL, the change in oxygen concentration during the ORR will be considered from the PEM-CCL interface $c_{O_2}^{'}$ to the CCL-GDL interface c_{eq,O_2}. The term that defines the change of oxygen concentration from the GDL-CCL interface to the PEM-CCL interface in the frequency domain (small disturbance of oxygen from the ac

perturbation) has already been developed in the authors' previous study [3] and will be considered in the next section.

The complex value of $\tilde{\gamma}_{PtO}$ can be related to $\tilde{V}$ if Eq. 10 is linearized by the following equation [19]:

$$nF\lambda\tilde{\gamma}_{PtO}\,j\omega=\left(\frac{\partial i_i}{\partial V}\right)_{ss}\tilde{V}+\left(\frac{\partial i_i}{\partial \gamma_{PtO}}\right)_{ss}\tilde{\gamma}_{PtO} \tag{19}$$

where ω is the angular frequency and j is the imaginary component.

Applying Eqs. 11 and 17 into Eqs. 19 and 18 and considering the oxygen concentration at the PEM-CCL interface $c_{O_2}=c_{O_2}^{'}$ yields:

$$\tilde{i}=\left[\frac{i_{0,O_2}b_{O_2}c_{O_2}^{'}\left(1-\gamma_{PtO,ss}\right)}{c_{eq,O_2}\left(1-\gamma_{eq,PtO,ss}\right)}\exp\left(-b_{O_2}\eta_{O_2,ss}\right)\right]\tilde{V}+\left[\frac{i_{0,O_2}c_{O_2}^{'}}{c_{eq,O_2}\left(1-\gamma_{eq,H_2O_2,ss}\right)}\exp\left(-b_{O_2}\eta_{O_2,ss}\right)\right]\tilde{\gamma}_{PtO} \tag{20}$$

$$nF\lambda\tilde{\gamma}_{PtO}\,j\omega=\left[\frac{i_{0,Pt}b_{Pt,f}\left(1-\gamma_{PtO,ss}\right)}{1-\gamma_{eq,PtO,ss}}\exp\left(b_{Pt,f}\eta_{Pt,ss}\right)+\frac{i_{0,Pt}b_{Pt,b}\gamma_{PtO,ss}}{\gamma_{eq,PtO,ss}}\exp\left(-b_{Ptb}\eta_{Pt,ss}\right)\right]\tilde{V}-\left[\frac{i_{0,Pt}}{1-\gamma_{eq,PtO,ss}}\exp\left(b_{Pt,f}\eta_{Pt,ss}\right)+\frac{i_{0,Pt}}{\gamma_{eq,PtO,ss}}\exp\left(-b_{Pt,b}\eta_{Pt,ss}\right)\right]\tilde{\gamma}_{PtO} \tag{21}$$

where the subscript *ss* represents the steady-state, $\eta_{i,ss}=V_{ss}-V_{eq,i,ss}$ is the overpotential at steady-state, $c_{O_2}^{'}$ is the oxygen concentration at the CCL-PEM interface, and c_{eq,O_2} is the concentration at the GDL-CCL interface.

The change in oxygen concentration across the CCL resulting from the small ac disturbance of the surface coverage of platinum oxide formation in the frequency domain $\tilde{\gamma}_{PtO}$ is considered negligible. Therefore, the ratio of oxygen concentration between the CCL-PEM and GDL-CCL interfaces $c_{O_2}^{'}/c_{eq,O_2}$, which are multiplied by $\tilde{\gamma}_{PtO}$ in Eq. 20 (second term on the right hand side), is considered to be steady-state. Under such considerations, it is possible to define Eqs. 20 and 21 in terms of charge transfer resistances and currents at the small disturbance of $\tilde{\gamma}_{PtO}$ from the ac perturbation:

$$\tilde{i}=\left[\frac{c_{O_2}^{'}}{c_{eq,O_2}}\frac{1}{R_{O_2}}\right]\tilde{V}+\left[i_{O_2,ss}\right]\tilde{\gamma}_{PtO} \tag{22}$$

$$nF\lambda\tilde{\gamma}_{PtO}\,j\omega=\left[\frac{1}{R_{Pt,f}}+\frac{1}{R_{Pt,b}}\right]\tilde{V}-\left[i_{Pt,f,ss}+i_{Pt,b,ss}\right]\tilde{\gamma}_{PtO} \tag{23}$$

where R_i represents the charge transfer resistance:

$$R_{O_2}=\frac{1-\gamma_{eq,PtO,ss}}{i_{0,O_2}b_{O_2}\exp\left(-b_{O_2}\eta_{O_2,ss}\right)\left(1-\gamma_{PtO,ss}\right)}\quad R_{Pt,b}=\frac{\gamma_{eq,PtO,ss}}{i_{0,Pt}b_{Pt,b}\exp\left(-b_{Ptb}\eta_{Pt,ss}\right)\gamma_{PtO,ss}}\quad R_{Pt,f}=\frac{1-\gamma_{eq,PtO,ss}}{i_{0,Pt}b_{Pt,f}\exp\left(b_{Pt,f}\eta_{Pt,ss}\right)\left(1-\gamma_{PtO,ss}\right)} \tag{24,25,26}$$

and $i_{i,ss}$ represents the current at the small disturbance of $\tilde{\gamma}_{PtO}$ from the ac perturbation:

$$i_{O_2,ss}=\frac{i_{0,O_2}c'_{O_2,ss}}{c_{eq,O_2,ss}\left(1-\gamma_{eq,PtO,ss}\right)}\exp\left(-b_{O_2}\eta_{O_2,ss}\right) \tag{27}$$

$$i_{Pt,f,ss}=\frac{i_{0,Pt}}{\left(1-\gamma_{eq,PtO,ss}\right)}\exp\left(b_{Pt,f}\eta_{Pt,ss}\right)\qquad i_{Pt,b,ss}=\frac{i_{0,Pt}}{\gamma_{eq,PtO,ss}}\exp\left(-b_{Pt,b}\eta_{Pt,ss}\right) \tag{28,29}$$

and $\gamma_{PtO,ss}$ represents the electrode surface coverage of platinum oxide at steady-state and can be calculated from Eq. 11 considering $d\gamma_{PtO}/dt=0$:

$$\gamma_{PtO,ss}=\frac{\frac{i_{0,Pt}}{\left(1-\gamma_{eq,PtO,ss}\right)}\exp\left(b_{Pt,f}\eta_{Pt,ss}\right)}{\frac{i_{0,Pt}}{\left(1-\gamma_{eq,PtO,ss}\right)}\exp\left(b_{Pt,f}\eta_{Pt,ss}\right)+\frac{i_{0,Pt}}{\left(\gamma_{eq,PtO,ss}\right)}\exp\left(-b_{Pt,b}\eta_{Pt,ss}\right)} \tag{30}$$

2.3 Oxygen transport limitations

The oxygen concentration at the electrode surface depends on the diffusion of oxygen through the multiphase via parallel and serial paths in the CCL [20]. In the authors' previous study [3] the ratio between oxygen concentrations at the CCL-PEM and CCL-GDL interfaces in the frequency domain was derived to characterise oxygen transport limitations in the impedance response of PEFCs. This ratio between oxygen concentrations is considered, as the EIS technique measures the change in oxygen concentration in the total CCL. This also allows the derivation of the Warburg Impedance which has been broadly used in the EIS area [21,22] to characterise oxygen transport limitations in the frequency domain during PEFC operation. The ratio of oxygen concentration at the PEM-CCL and GDL-CCL interface at the frequency domain is expressed as [3]:

$$\frac{c'_{O_2}}{c_{eq,O_2}}=\frac{R_{O_2}}{R_{O_2}+Z_W} \tag{31}$$

where R_{O_2} is the charge transfer resistance for the oxygen reduction which can be represented through Eq. 24 and

$$Z_W=R_W\frac{\tanh\left(j\omega T_W\right)^{0.5}}{\left(j\omega T_W\right)^{0.5}} \tag{32}$$

is known as the Warburg Impedance [21,22] and characterises oxygen transport limitations in EIS measurements of PEFCs, with

$$R_W = \frac{RT\delta}{n^2 F^2 c_{eq,O_2} D} \tag{33}$$

defined as the resistance of the diffusion process and

$$T_W = \frac{\delta^2}{D} \tag{34}$$

defined as the time constant to diffuse oxygen through the CCL.

3. Electrochemical Impedance of the PEFC under platinum oxidation

Substituting Eq. 31 into Eq. 22 gives:

$$\tilde{i} = \left[\frac{1}{R_{O_2} + Z_W}\right]\tilde{V} + \left[i_{O_2,ss}\right]\tilde{\gamma}_{PtO} \tag{35}$$

Arranging Eq. 23 for $\tilde{\gamma}_{PtO}$ yields:

$$\tilde{\gamma}_{PtO} = \left[\frac{R_{Pt,f} + R_{Pt,b}}{R_{Pt,f} R_{Pt,b}\left(nF\lambda j\omega + i_{Pt,f,ss} + i_{Pt,b,ss}\right)}\right]\tilde{V} \tag{36}$$

Substituting Eq. 36 into Eq. 35 yields:

$$\tilde{i} = \left[\frac{1}{R_{O_2} + Z_W} + \frac{i_{O_2,ss}\left(R_{Pt,f} + R_{Pt,b}\right)}{R_{Pt,f} R_{Pt,b}\left(nF\lambda j\omega + i_{Pt,f,ss} + i_{Pt,b,ss}\right)}\right]\tilde{V} \tag{37}$$

The CCL is formed by a double layer structure of the interface between dissimilar materials, i.e., the electrode-electrolyte interface. The electrode represents the electron-conducting network of carbon-supported platinum agglomerates while the electrolyte represents the ion-conducting dispersion of Nafion. At this interface an electric field is present and has a determinant role in the charge distribution within the reactants as well as in the position and orientation of the reactant to form the desired products. This double layer can behave like a capacitor that is in parallel with the electrode reactions; the current passing from the electrode to the electrolyte can either take part in the charge transfer reactions or contribute to the charge in the capacitive effect. The electrochemical reaction in the electrode results in an inhomogeneous distribution of charge in the catalyst layer. As a result, a non-ideal capacitor (Constant Phase Element) [23] defined in the frequency domain $j\omega$ has to be considered in the theoretical treatment, in order to correct for this inhomogeneity:

$$\tilde{i} = \left[\frac{1}{R_{O_2} + Z_W} + \frac{i_{O_2,ss}\left(R_{Pt,f} + R_{Pt,b}\right)}{R_{Pt,f} R_{Pt,b}\left(nF\lambda j\omega + i_{Pt,f,ss} + i_{Pt,b,ss}\right)} \right] \tilde{V} + Y(j\omega)^P \tilde{V} \tag{38}$$

where Y represents a parameter related to capacitance and superscript P represents a parameter to correct the inhomogeneity in the distribution of charge.

Eq. 38 can be rearranged to express the electrical current that enters a circuit composed of resistive, inductive and capacitive elements, as shown in Fig. 1

giving:

$$\tilde{i} = \left[\frac{1}{R_{O_2} + Z_W} + \frac{1}{(\tau_{PtO} j\omega + 1) R_{PtO}} + Y(j\omega)^P \right] \tilde{V} \tag{39}$$

where

$$\tau_{PtO} = \frac{L}{R_{PtO}} = \frac{nF\lambda}{i_{Pt,f,ss} + i_{Pt,b,ss}}, \quad R_{PtO} = \frac{R_{Pt,f} R_{Pt,b}\left(i_{Pt,f,ss} + i_{Pt,b,ss}\right)}{\left(R_{Pt,f} + R_{Pt,b}\right) i_{O_2,ss}}$$

characterise inductive loops at low frequencies in the impedance response of PEFCs, τ_{PtO} and R_{PtO} are the time constant and resistance for platinum oxidation rate.

Rearranging Eq. 39 yields the electrochemical impedance of the cathode accounting for platinum oxidation during the ORR:

$$Zc_{PtO} = \left[\frac{1}{\frac{1}{R_{O_2} + Z_W} + \frac{1}{(\tau_{PtO} j\omega + 1) R_{PtO}} + Y(j\omega)^P} \right] \tag{40}$$

The hydrogen oxidation reaction (HOR) mechanisms occurring at the anode have been proposed by Malevich *et al.* [21] to be represented as an electrical circuit composed of a resistor (charge transfer resistance) in parallel with a capacitor (representing the double layer capacitance). HOR taking place in the anode is a faster and a less complicated reaction sequence than the ORR in the cathode and can be represented in the frequency domain as:

$$Za = \frac{Ra}{1 + j\omega RaCa} \tag{41}$$

if no contaminants such as CO are present, where Ra is charge transfer resistance and Ca is capacitance.

The opposition of ions flowing through the PEM, and electrons flowing through the bipolar plate and GDL can be represented by resistances connected in series. The overall process can be represented with a total resistance $Rohm$ that accounts for the different resistances in the layers of the PEFC.

Therefore, the impedance of the PEFC including anode, cathode, and PEM can be represented through the following equation:

$$Z_{FC,C_{PtO}} = Rohm + Za + Zc_{PtO} \tag{42}$$

where R_{ohm} represents the ohmic resistance of the PEM, bipolar plates, GDL, the second term on the right hand side represents Eq. 41 and the third term represents the cathode impedance (Eq. 40). Eq. 42 can be represented through the equivalent electrical circuit shown in Fig. 2.

4. Experimental Validation for Platinum Oxide Model

In the authors' previous study [7] an impedance model based on electrochemistry of hydrogen peroxide formation during the ORR was developed. The model predicted that inductive loops at low frequencies of the impedance spectrum are related to kinetics of hydrogen peroxide formation. In this study, the experimental EIS measurements, which feature inductive loops, reported in the authors' previous studies [7,8] were considered to validate the impedance model that predicts platinum oxidation during the ORR, as it has been proposed that platinum oxidation mechanisms could also be represented as inductive loops at low frequencies [4,6]. The reason for validating the current theoretical treatment with the EIS measurements reported in the previous study [7,8] is due to the slight difference in the shape of the inductive loop from experimental data compared to the simulated data from the model predicting hydrogen peroxide formation [7]. This difference could reveal that not only hydrogen peroxide formation is present in the EIS measurements but also platinum oxidation that can cause lower fuel cell performance. The EIS measurements were carried out in a 4-cell open-cathode PEFC stack at 0.1875, 0.3125, and 0.4375 A/cm^2 and at frequencies from 10 kHz down to 0.1 Hz, with a 5% AC amplitude of the DC current. The DC polarisation resistance which is calculated through the slope of the polarisation curve and is related to EIS measurements when the frequency is decreased near zero [24] was calculated for the three current densities. Fig. 3 shows a graphical interpretation to calculate the DC polarisation resistance at current density of 0.3125 A/cm^2 through the polarisation curve of the 4-cell open-cathode PEFC stack.

The electrical circuit shown in Fig. 2 which simulates the impedance response of the PEFC under platinum oxide formation was constructed in ZView software (Scribner Associates, Inc). The electrical circuit was fitted to the EIS measurements through a complex nonlinear regression method (Levenberg-Marquardt). The parameters of electrical circuit (Eq. 42) extracted from the measured EIS data are shown in Table I.

At a current density of 0.3125 A/cm^2 there is a decrease in the impedance spectrum and an increase in the spectrum at 0.4375 A/cm^2, as shown in Fig. 4. This is consistent with the results shown in Table I if we consider the sum of charge transfer resistance R_{O_2} and mass transport resistance R_W during ORR. The reduction and increase of the spectrum at 0.3125 A/cm^2 and 0.4375 A/cm^2 respectively has been discussed in the authors' previous study [7,8] and supported by experimental results reported in other studies [25,26]. The comparison between experimental and simulated data shown in Fig. 4 demonstrates that the impedance model to predict the rate of platinum oxidation cannot accurately reproduce the inductive loop at low frequencies. In the authors' previous study [7] an impedance model to predict hydrogen peroxide formation during the ORR was validated with the experimental EIS measurements present in this study. The previous model could not predict accurately the low frequency loops either (Fig. 6 Ref. [7]). Each model (hydrogen peroxide formation and platinum oxidation) predicted a time constant for the corresponding electrochemical mechanisms. Also the models predict a different polarisation resistance *Rp* which is related to the slope of the polarisation curve (≈ 2.5 Ω.cm^2 at 0.3125 A/cm^2 based on Fig. 3) when the frequency is decreased, e.g. 1 μ Hz, as shown in Fig. 4. It seems that the inductive loops from the experimental EIS measurements are formed by more than one time constant representing different electrochemical mechanisms. As different mechanisms that cause low performance and degradation can be simultaneously present during PEFC operation, in the next section an impedance model that considers hydrogen peroxide formation in combination with platinum oxidation will be developed.

5. Cathode Impedance model considering Platinum Oxide and Hydrogen Peroxide kinetics

It was not possible to simulate the inductive loop of the EIS measurements and relate the DC polarisation resistance at low frequencies using the impedance model accounted for Hydrogen Peroxide, developed in the author's previous study [7], nor with the impedance model for platinum oxidation developed in this study. The reason for each model not being able to reproduce the inductive loop in the EIS measurements could be related

to the fact that the inductive loop is not a result of a single time constant electrochemical mechanism. The two-step ORR which yields the formation of hydrogen peroxide (H_2O_2) and the formation of water (H_2O) was expressed in a previous study [7] as:

$$O_2 + 2H^+ + 2e^- \xrightarrow{k1} H_2O_2 \tag{43}$$

$$H_2O_2 + 2H^+ + 2e^- \xrightarrow{k2} 2H_2O \tag{44}$$

In this study, it is considered that the rate of reactions (43) and (44) is affected by the rate of Platinum oxide formation expressed in reaction (1), therefore the current densities corresponding to reactions (43) and (44) can be expressed in terms of the fractional surface coverage of Platinum oxide as:

$$i_{O_2} = -nFk_1 c_{O_2} c_{eq,H^+}^{3/2} \left(1-\gamma_{H_2O_2}\right)\left(1-\gamma_{PtO}\right)\exp\left(-b_{O_2}V\right) \tag{45}$$

$$i_{H_2O_2} = -nFk_2 c_{eq,H_2O_2} c_{eq,H^+}^{3/2} \gamma_{H_2O_2}\left(1-\gamma_{PtO}\right)\exp\left(-b_{H_2O_2}V\right) \tag{46}$$

where $\gamma_{H_2O_2}$ is the fractional surface coverage of hydrogen peroxide, and $c_{eq,i}$ represents the concentration at equilibrium conditions as it is assumed that surface concentration of protons and hydrogen peroxide is constant.

If the fractional surface coverage of platinum oxide γ_{PtO} increases, the currents related to the two-step ORR (Eqs. 45 and 46) become less negative. Eqs. 45 and 46 can be expressed considering exchange currents as:

$$i_{O_2} = -i_{0,O_2} \frac{c_{O_2}}{c_{eq,O_2}} \frac{\left(1-\gamma_{H_2O_2}\right)\left(1-\gamma_{PtO}\right)}{\left(1-\gamma_{eq,H_2O_2}\right)\left(1-\gamma_{eq,PtO}\right)} \exp\left[-b_{O_2}\left(V-V_{eq,O_2}\right)\right] \tag{47}$$

$$i_{H_2O_2} = -i_{0,H_2O_2} \frac{\gamma_{H_2O_2}\left(1-\gamma_{PtO}\right)}{\gamma_{eq,H_2O_2}\left(1-\gamma_{eq,PtO}\right)} \exp\left[-b_{H_2O_2}\left(V-V_{eq,H_2O_2}\right)\right] \tag{48}$$

With

$$i_{0,O_2} = nFk_1 c_{eq,O_2} c_{eq,H^+}^{3/2} \left(1-\gamma_{eq,H_2O_2}\right)\left(1-\gamma_{eq,PtO}\right)\exp\left(-b_{O_2}V_{eq,O_2}\right) \tag{49}$$

$$i_{0,H_2O_2} = nFk_2 c_{eq,H_2O_2} c_{eq,H^+}^{3/2} \gamma_{eq,H_2O_2}\left(1-\gamma_{eq,PtO}\right)\exp\left(-b_{H_2O_2}V_{eq,H_2O_2}\right) \tag{50}$$

where Eqs. 49 and 50 are the exchange current densities for reactions (43) and (44) considering the fractional surface coverage of platinum oxide.

The total current for the two-step ORR is defined as $i = i_{O_2} + i_{H_2O_2}$:

$$i = -i_{0,O_2} \frac{c_{O_2}}{c_{eq,O_2}} \frac{\left(1-\gamma_{H_2O_2}\right)\left(1-\gamma_{PtO}\right)}{\left(1-\gamma_{eq,H_2O_2}\right)\left(1-\gamma_{eq,PtO}\right)} \exp\left[-b_{O_2}\left(V-V_{eq,O_2}\right)\right] - i_{0,H_2O_2} \frac{\gamma_{H_2O_2}\left(1-\gamma_{PtO}\right)}{\gamma_{eq,H_2O_2}\left(1-\gamma_{eq,PtO}\right)} \exp\left[-b_{H_2O_2}\left(V-V_{eq,H_2O_2}\right)\right] \tag{51}$$

The variation rate of $\gamma_{H_2O_2}$ with respect to time can be defined as in the previous study [7] as:

$$nF\beta\frac{d\gamma_{H_2O_2}}{dt}=-i_{0,O_2}\frac{c_{O_2}}{c_{eq,O_2}}\frac{\left(1-\gamma_{H_2O_2}\right)\left(1-\gamma_{PtO}\right)}{\left(1-\gamma_{eq,H_2O_2}\right)\left(1-\gamma_{eq,PtO}\right)}\exp\left[-b_{O_2}\left(V-V_{eq,O_2}\right)\right]+i_{0,H_2O_2}\frac{\gamma_{H_2O_2}\left(1-\gamma_{PtO}\right)}{\gamma_{eq,H_2O_2}\left(1-\gamma_{eq,PtO}\right)}\exp\left[-b_{H_2O_2}\left(V-V_{eq,H_2O_2}\right)\right] \tag{52}$$

where β is the maximum surface coverage by hydrogen peroxide.

The variation of γ_{PtO} with respect to time has been defined in Eq. 11.

5.1 ac impedance response

A linear model for current resulting from a small ac perturbation and using Taylor series expansion is represented as:

$$\tilde{i}=\left(\frac{\partial i}{\partial V}\right)_{ss}\tilde{V}+\left(\frac{\partial i}{\partial\gamma_{H_2O_2}}\right)_{ss}\tilde{\gamma}_{H_2O_2}+\left(\frac{\partial i}{\partial\gamma_{PtO}}\right)_{ss}\tilde{\gamma}_{PtO} \tag{53}$$

Similar to Eq. 18 the small disturbance of oxygen from the ac perturbation is not considered in Eq. 53 at first as a priori decoupling between oxygen transport limitations and surface coverage is considered. Thereafter the Warburg impedance, which has been broadly used in the analysis of oxygen transport limitations in experimental EIS measurements, will be incorporated in the mathematical treatment to account for the small disturbance of oxygen from the ac perturbation. Also the change in oxygen concentration during the ORR will be considered from the PEM-CCL interface c'_{O_2} to the CCL-GDL interface c_{eq,O_2}.

The complex value of $\tilde{\gamma}_{H_2O_2}$ can be related to $\tilde{V}$ if Eq. 52 is linearized by the following equation [19]:

$$nF\beta\tilde{\gamma}_{H_2O_2}\,j\omega=\left(\frac{\partial i_i}{\partial V}\right)_{ss}\tilde{V}+\left(\frac{\partial i_i}{\partial\gamma_{H_2O_2}}\right)_{ss}\tilde{\gamma}_{H_2O_2} \tag{54}$$

Noting that $\tilde{\gamma}_{PtO}$ is not considered in Eq. 54. γ_{PtO} is considered at steady state in Eq. 54. This consideration will allow decoupling *PtO* and H_2O_2 mechanisms during the ac perturbation. Applying Eq. 51 into Eq. 53, and Eq. 52 into Eq. 54, yields:

$$\begin{aligned}\tilde{i}=&\left[\frac{i_{0,O_2}b_{O_2}c'_{O_2}\left(1-\gamma_{H_2O_2,ss}\right)\left(1-\gamma_{PtO,ss}\right)}{c_{eq,O_2}\left(1-\gamma_{eq,H_2O_2,ss}\right)\left(1-\gamma_{eq,PtO,ss}\right)}\exp\left(-b_{O_2}\eta_{O_2,ss}\right)+\frac{i_{0,H_2O_2}b_{H_2O_2}\gamma_{H_2O_2,ss}\left(1-\gamma_{PtO,ss}\right)}{\gamma_{eq,H_2O_2,ss}\left(1-\gamma_{eq,PtO,ss}\right)}\exp\left(-b_{H_2O_2}\eta_{H_2O_2,ss}\right)\right]\tilde{V}\\&+\left[\frac{i_{0,O_2}c'_{O_2}\left(1-\gamma_{PtO,ss}\right)}{c_{eq,O_2}\left(1-\gamma_{eq,H_2O_2,ss}\right)\left(1-\gamma_{eq,PtO,ss}\right)}\exp\left(-b_{O_2}\eta_{O_2,ss}\right)-\frac{i_{0,H_2O_2}\left(1-\gamma_{PtO,ss}\right)}{\gamma_{eq,H_2O_2,ss}\left(1-\gamma_{eq,PtO,ss}\right)}\exp\left(-b_{H_2O_2}\eta_{H_2O_2,ss}\right)\right]\tilde{\gamma}_{H_2O_2}\\&+\left[\frac{i_{0,O_2}c'_{O_2}\left(1-\gamma_{H_2O_2,ss}\right)}{c_{eq,O_2}\left(1-\gamma_{eq,H_2O_2,ss}\right)\left(1-\gamma_{eq,PtO,ss}\right)}\exp\left(-b_{O_2}\eta_{O_2,ss}\right)+\frac{i_{0,H_2O_2}\gamma_{H_2O_2,ss}}{\gamma_{eq,H_2O_2,ss}\left(1-\gamma_{eq,PtO,ss}\right)}\exp\left(-b_{H_2O_2}\eta_{H_2O_2,ss}\right)\right]\tilde{\gamma}_{PtO}\end{aligned} \tag{55}$$

$$nF\beta\tilde{\gamma}_{H_2O_2}\,j\omega=\left[\frac{i_{0,O_2}b_{O_2}c'_{O_2}\left(1-\gamma_{H_2O_2,ss}\right)\left(1-\gamma_{PtO,ss}\right)}{c_{eq,O_2}\left(1-\gamma_{eq,H_2O_2,ss}\right)\left(1-\gamma_{eq,PtO,ss}\right)}\exp\left(-b_{O_2}\eta_{O_2,ss}\right)-\frac{i_{0,H_2O_2}b_{H_2O_2}\gamma_{H_2O_2,ss}\left(1-\gamma_{PtO,ss}\right)}{\gamma_{eq,H_2O_2,ss}\left(1-\gamma_{eq,PtO,ss}\right)}\exp\left(-b_{H_2O_2}\eta_{H_2O_2,ss}\right)\right]\tilde{V}$$

$$+\left[\frac{i_{0,O_2}c'_{O_2}\left(1-\gamma_{PtO,ss}\right)}{c_{eq,O_2}\left(1-\gamma_{eq,H_2O_2,ss}\right)\left(1-\gamma_{eq,PtO,ss}\right)}\exp\left(-b_{O_2}\eta_{O_2,ss}\right)+\frac{i_{0,H_2O_2}\left(1-\gamma_{PtO,ss}\right)}{\gamma_{eq,H_2O_2,ss}\left(1-\gamma_{eq,PtO,ss}\right)}\exp\left(-b_{H_2O_2}\eta_{H_2O_2,ss}\right)\right]\tilde{\gamma}_{H_2O_2} \tag{56}$$

The change in oxygen concentration across the CCL resulting from the small ac disturbance of the surface coverage of platinum oxide formation $\tilde{\gamma}_{PtO}$ and from the small ac disturbance of the surface coverage of hydrogen peroxide formation $\tilde{\gamma}_{H_2O_2}$ in the frequency domain is considered negligible. Therefore, the ratio of oxygen concentration between the CCL-PEM and GDL-CCL interfaces $c'_{O_2}/c_{eq,O_2}$, which are multiplied by $\tilde{\gamma}_{PtO}$ and $\tilde{\gamma}_{H_2O_2}$ in Eqs. 55 and 56 is considered to be steady-state. Eq. 55 and 56 can be rearranged and expressed in terms of charge transfer resistances and currents at the small disturbance of $\tilde{\gamma}_{PtO}$ and $\tilde{\gamma}_{H_2O_2}$ from the ac perturbation :

$$\tilde{i}=\left[\frac{1}{R_{O_2}}\frac{c'_{O_2}}{c_{eq,O_2}}+\frac{1}{R_{H_2O_2}}\right]\tilde{V}+\left[i_{H_2O_2,\gamma_{Pto,ss}}-i_{O_2,\gamma_{Pto,ss}}\right]\tilde{\gamma}_{H_2O_2}+\left[i_{O_2,ss}+i_{H_2O_2,ss}\right]\tilde{\gamma}_{PtO} \tag{57}$$

$$nF\beta\tilde{\gamma}_{H_2O_2}\,j\omega=\left[\frac{c'_{O_2}}{c_{eq,O_2}}\frac{1}{R_{O_2}}-\frac{1}{R_{H_2O_2}}\right]\tilde{V}-\left[i_{O_2,\gamma_{Pto,ss}}+i_{H_2O_2,\gamma_{Pto,ss}}\right]\tilde{\gamma}_{H_2O_2} \tag{58}$$

where R_i represents the charge transfer resistance

$$R_{O_2}=\frac{\left(1-\gamma_{eq,H_2O_2,ss}\right)\left(1-\gamma_{eq,PtO,ss}\right)}{i_{0,O_2}b_{O_2}\exp\left(-b_{O_2}\eta_{O_2,ss}\right)\left(1-\gamma_{H_2O_2,ss}\right)\left(1-\gamma_{PtO,ss}\right)} \qquad R_{H_2O_2}=\frac{\gamma_{eq,H_2O_2,ss}\left(1-\gamma_{eq,PtO,ss}\right)}{i_{0,H_2O_2}b_{H_2O_2}\exp\left(-b_{H_2O_2}\eta_{H_2O_2,ss}\right)\gamma_{H_2O_2,ss}\left(1-\gamma_{PtO,ss}\right)} \tag{59,60}$$

$i_{i,\gamma_{Pto,ss}}$ represents the current considering the fractional surface coverage of platinum oxide at steady state at the small disturbance of $\tilde{\gamma}_{H_2O_2}$ from the ac perturbation, and $i_{i,ss}$ represents the current at the small disturbance of $\tilde{\gamma}_{PtO}$ from the ac perturbation.

Substituting Eqs. 31, 36 and 58 into Eq. 57 yields:

$$\tilde{i}=\left[\frac{1}{R_{O_2}+Z_W}+\frac{1}{R_{H_2O_2}}\right]\tilde{V}+\left[\frac{\left(i_{H_2O_2,\gamma_{Pto,ss}}-i_{O_2,\gamma_{Pto,ss}}\right)\left(R_{H_2O_2}-R_{O_2}-Z_W\right)}{R_{H_2O_2}\left(R_{O_2}+Z_W\right)\left(nF\beta j\omega+i_{H_2O_2,\gamma_{Pto,ss}}+i_{O_2,\gamma_{Pto,ss}}\right)}\right]\tilde{V}+\left[\frac{\left(i_{O_2,ss}+i_{,H_2O_2,ss}\right)\left(R_{Pt,f}+R_{Pt,b}\right)}{R_{Pt,f}R_{Pt,b}\left(nF\lambda j\omega+i_{Pt,f,ss}+i_{Pt,b,ss}\right)}\right]\tilde{V} \tag{61}$$

Similar to Eq. 38, a non-ideal capacitor (Constant Phase Element) defined in the frequency domain $j\omega$ to correct for the inhomogeneity in the distribution of charge between the electrode-electrolyte interface in the electrode is considered [23]:

$$\tilde{i}=\left[\frac{1}{R_{O_2}+Z_W}+\frac{1}{R_{H_2O_2}}\right]\tilde{V}+\left[\frac{\left(i_{H_2O_2,\gamma_{PtO},ss}-i_{O_2,\gamma_{PtO},ss}\right)\left(R_{H_2O_2}-R_{O_2}-Z_W\right)}{R_{H_2O_2}\left(R_{O_2}+Z_W\right)\left(nF\beta j\omega+i_{H_2O_2,\gamma_{PtO},ss}+i_{O_2,\gamma_{PtO},ss}\right)}\right]\tilde{V}+\left[\frac{\left(i_{O_2,ss}+i_{,H_2O_2,ss}\right)\left(R_{Pt,f}+R_{Pt,b}\right)}{R_{Pt,f}R_{Pt,b}\left(nF\lambda j\omega+i_{Pt,f,ss}+i_{Pt,b,ss}\right)}\right]\tilde{V}+Y\left(j\omega\right)^P\tilde{V} \quad (62)$$

Eq. 62 can be expressed as the current that enters to an electrical circuit:

$$\tilde{i}=\left[\frac{1}{R_{O_2}+Z_W}+\frac{1}{R_{H_2O_2}}\right]\tilde{V}+\left[A\phi_{H_2O_2}\right]\tilde{V}+\left[\frac{1}{\left(\tau_{PtO}\,j\omega+1\right)R_{PtO}}\right]\tilde{V}+Y\left(j\omega\right)^P\tilde{V} \quad (63)$$

where

$$A\phi_{H_2O_2}=\frac{1}{\left(\tau_{H_2O_2}\,j\omega+1\right)R\phi_{H_2O_2}},\quad \tau_{H_2O_2}=\frac{nF\beta}{i_{H_2O_2,\gamma_{PtO},ss}+i_{O_2,\gamma_{PtO},ss}},\quad R\phi_{H_2O_2}=\frac{R_{H_2O_2}\left(R_{O_2}+Z_W\right)\left(i_{H_2O_2,\gamma_{PtO},ss}+i_{O_2,\gamma_{PtO},ss}\right)}{\left(R_{H_2O_2}-R_{O_2}-Z_W\right)\left(i_{H_2O_2,\gamma_{PtO},ss}-i_{O_2,\gamma_{PtO},ss}\right)},$$

$\tau_{H_2O_2}$ and $R\phi_{H_2O_2}$ are the time constant and resistance for hydrogen peroxide formation, and

$$\tau_{PtO}=\frac{L}{R_{PtO}}=\frac{nF\lambda}{i_{Pt,f,ss}+i_{Pt,b,ss}},\quad R_{PtO}=\frac{\left(R_{Pt,f}R_{Pt,b}\right)\left(i_{Pt,f,ss}+i_{Pt,b,ss}\right)}{\left(R_{Pt,f}+R_{Pt,b}\right)\left(i_{O_2,ss}+i_{,H_2O_2,ss}\right)}$$

τ_{PtO} and R_{PtO} are the time constant and resistance for platinum oxide formation.

Rearranging Eq. 63 yields the electrochemical impedance of the cathode accounting for hydrogen peroxide and platinum oxide formation during the ORR:

$$Zc_{H_2O_2,PtO}=\left[\frac{1}{\frac{1}{R_{O_2}+Z_W}+\frac{1}{R_{H_2O_2}}+A\phi_{H_2O_2}+\frac{1}{\left(\tau_{PtO}\,j\omega+1\right)R_{PtO}}+Y\left(j\omega\right)^P}\right] \quad (64)$$

Combining Eq. 41, Eq. 64 and considering the Ohmic resistance of the PEFC, yields the impedance of the PEFC considering hydrogen peroxide and platinum oxide formation at the cathode.

$$Z_{FC,C_{H_2O_2,PtO}}=Rohm+Za+Zc_{H_2O_2,PtO} \quad (65)$$

Eq. 65 can be represented through the circuit shown in Fig. 5. Noting that circuit shown in Fig. 5 is the combination of electrical circuits representing the impedance of the PEFC considering hydrogen peroxide formation (Fig. 2 from previous study [7]) and platinum oxide formation (Fig. 2). The parameters of the circuit shown in Fig. 5 such as R_{PtO} and $R\phi_{H_2O_2}$ are a function of the rate of *PtO* and H_2O_2 respectively.

6. Experimental Validation for Hydrogen Peroxide with Platinum Oxide Model

In the author's previous study [8] EIS measurements were carried out in individual cells of a 4-cell Open cathode PEFC stack using a multichannel frequency response analyser (Z#106 WonATech Co). The results demonstrated (Figs. 3, 4 and 5 from previous study [8]) that one cell showed a difference in impedance response compared to the rest of the cells at frequencies from 10 kHz to 100 Hz. The charge transfer phenomenon between electrode-electrolyte interface is commonly represented at this frequency range [27]. This difference in impedance response could be accounted to a loss in active area and therefore a decrease in performance in the MEA of that particular cell. As a hypothesis, it is considered that production of hydrogen peroxide and platinum oxide may have contributed to the decrease in performance. Meyer *et al.* [28] reported that inductive loops in EIS measurements carried out in an Open-cathode stack are related to side reactions (e.g. hydrogen peroxide, platinum oxide) during the ORR. In this study, the impedance model that accounts for the production of hydrogen peroxide and platinum oxide formation is validated with the EIS results of the 4-cell Open cathode PEFC stack reported in previous studies [7,8]. It was not possible to construct the entire model shown in Fig. 5 in Zview software as the component $A\phi_{H_2O_2}$ is an analytical expression and a frequency dependent parameter, therefore it cannot be expressed as a resistor in Zview software. To validate the impedance model expressed in Eq. 65, first the component $A\phi_{H_2O_2}$ from the electrical circuit shown in Fig. 5 was removed and the resulting circuit was constructed in Zview and fitted to the EIS measurements, as shown in Fig. 6a.

Thereafter the component $A\phi_{H_2O_2}$ was fitted to the EIS measurements using a Graphic User Interface (GUI) developed in Matlab and considering the values of the parameters previously estimated through Zview software. The least squares fitting method was used in order to find the best-fit between the model and the measured data. A good quality fit is obtained when the sum of the deviations squared (least square error) between the simulated and measured impedance data has a minimum value, for instance <0.1. The parameters of Eq. 65 extracted from the measured EIS data are shown in Table II.

Fig. 7 demonstrates that it is possible to accurately reproduce the inductive loop at low frequencies of the EIS measurements at the three current densities through Eq. 65 and the parameters shown in Table II. Fig. 7 also shows that it is possible to extrapolate and simulate the EIS data using Eq. 65 at a minimum frequency of 1 μHz to calculate the DC polarisation resistance. Impedance models reported in the literature [4,6,29] have extrapolated the inductive loop by reducing frequency to find the DC polarisation resistance. Inductive loops

have not been experimentally validated at the lowest frequency range (e.g 1 μHz), because it is not practical to wait such a long time to carry out EIS measurements under such a frequency range [28]. Fig. 7 demonstrates that the polarisation resistance calculated at a frequency of 1 μHz is in agreement with the polarisation resistance calculated from the polarisation curve (≈ 2.53 $\Omega.cm^2$ at 0.3125 A/cm^2) shown in Fig. 3. A recently study carried out by Chandesris *et al.* [30] reported that there is no difference between the low frequency resistance of EIS measurements and the direct current resistance from the slope of a polarisation curve when the polarisation curves are performed at constant air flow rate. The authors also reported that the difference is observed when the polarisation curve is performed at constant air stoichiometry. In this study, the EIS measurements and polarisation curve carried out in the open-cathode stack were performed at constant air flow rate (constant fan speed). Therefore as reported by Chandesris *et al.* [30] there is no difference between the resistance at low frequency limit (Fig. 7) and the DC polarisation resistance (Fig. 3).

The simulation results from 0.1 Hz to 1 μHz reveal the presence of a second time constant in the inductive loop. Antaño-Lopez *et al.* [31] reported EIS measurements carried out for anodic dissolution of iron in a molar sulfate solution at pH4. EIS measurements featured two inductive loops at low frequencies which are related to the relaxation of the surface coverage by two adsorbed Fe(I) intermediates involved in the dissolution mechanisms. Similar mechanisms in EIS measurements have been reported by Keddam *et al.* [32]. Eq. 65 predicts that two inductive loops are present in the EIS measurements, one related to hydrogen peroxide formation and the second related to platinum oxide formation at the lowest frequencies. A comparison in Bode format between the model and experimental results as shown in Figs 8, 9 demonstrates that the model can predict the experimental measurements under the operating frequency range tested.

Results and Discussion

Table II shows that the charge transfer resistance related to ORR R_{O_2} decreases with increasing current density. The charge transfer resistance reflects the increase in the driving force for the interfacial oxygen-reduction process [33]. A decrease in charge transfer resistance during ORR with increasing current in EIS measurements has been reported by Yuan *et al.* [25] and Paganin *et al.* [26]. Table II also shows an increase in the oxygen diffusion resistance R_W with increasing current density. The increase in oxygen diffusion resistance can be related to an increase in water product concentration with increasing current which impedes oxygen molecules to reach the active sites of the CCL [33]. The parameter R_{PtO} which is related to the resistance for platinum

oxide formation and contributes to the inductive loop at low frequencies decreases with increasing the current density. The decrease of R_{PtO} which yields an increase of platinum oxide can be related to an increase in water concentration during the ORR, as reported in literature [11,14].The results shown in Table II also demonstrate that the resistance for hydrogen peroxide formation $R_{H_2O_2}$ is higher than the resistance of platinum oxide formation R_{PtO}. The magnitude of time constants for such mechanisms $\tau_{PtO} > \tau_{H_2O_2}$ also demonstrates that the rate of platinum oxide formation is slower than the rate of hydrogen peroxide formation. Hence the mechanism that mainly contributes to low performance in the open-cathode stack, which the EIS measurements are related to, are mainly attributed to platinum oxide formation during PEFC operation. Roy *et al.* [4] developed independent impedance models considering hydrogen peroxide formation and platinum dissolution to study inductive loops in EIS measurements. Although recent studies [6,9] have moved onto focus on the role of platinum oxide on Inductive loops. This study has demonstrated that different mechanisms that can cause low performance and degradation in PEFCs can be simultaneously represented in EIS measurements.

The effect of oxygen diffusion resistance on the impedance response is discussed as follows. Three different cases as shown in Figs. 10a,b,c at different oxygen diffusion resistance R_W in Eq. 65 are considered. As a base case, the parameters represented in Table II at 0.3125 A/cm^2 are considered. In the first case, the impedance response is simulated when oxygen diffusion resistance is decreased from 2.6302 to 1.6302 Ω.cm^2 and the rest of the parameters in Eq. 65 are kept unchanged. Fig. 10a shows that it is possible to identify the two inductive loops related to hydrogen peroxide formation and platinum oxidation in which the second inductive loop at low frequencies is related to platinum oxidation. One of the disadvantages of the EIS technique is that the frequency dependency is obscured because multiple energy controlled processes of an electrochemical system can be masked in the frequency plot [33]. The time constants related to hydrogen peroxide formation, platinum oxidation and oxygen transport limitations at low frequencies can be overlapped in the complex-impedance plot. In the second case shown in fig. 10b the oxygen diffusion resistance is increased from 2.6302 to 3.2302 Ω.cm^2 and the rest of the parameters in Eq. 65 are unchanged; therefore the impedance response related to hydrogen peroxide formation becomes capacitive and the low frequency inductive loop at low frequencies is only related to platinum oxidation. In the authors' previous study [7] it was demonstrated that if the charge transfer resistance related to hydrogen peroxide reaction $R_{H_2O_2}$ is smaller than the sum of charge transfer resistance and Warburg resistance accounting for oxygen diffusion resistance $R_{O_2} + Z_W$ during the first-step ORR, a

capacitive loop at low frequencies is predicted instead of the inductive loop related to hydrogen peroxide formation during the ORR. Fig. 10b demonstrates that if oxygen diffusion resistance is increased, then the relation $R_{H_2O_2} < R_{O_2} + Z_W$ is complied with and yields to the capacitive loop for hydrogen peroxide formation. In the third case, as shown in Fig. 10c, the oxygen diffusion resistance is gradually decreased from the base case 2.6302 to 1.6302 and 0.6302, $\Omega.cm^2$ and the analytical expression related to PtO formation in Eq. 65 is neglected; therefore the inductive loop related to hydrogen peroxide increases with decreasing oxygen diffusion resistance until no further change in the inductive loop is observed. This effect can be related to the overlapping between hydrogen peroxide formation and oxygen transport mechanisms on the impedance plot as discussed through Fig. 10a. As expected, the results in Figs. 10a,b,c demonstrate that the DC polarisation resistance related to the slope of the polarisation curve as frequency reaches zero decreases with decreasing oxygen transport limitations.

High concentration of water produced during the ORR or high relative humidity enhances the conduction of protons through the MEA and catalyst layer. Nevertheless high water concentration hinders the diffusion of oxygen through the porous media in the GDL and CCL to reach the active sites in the CCL. As demonstrated in the literature [11] water concentration and high relative humidity increases the rate of platinum oxidation which eventually can yield a loss of active area in the cathode electrode. This demonstrates how complicated is the balance between the physical processes occurring in the PEFC to achieve high performance and durability.

7. Conclusion

An impedance model that accounts for platinum oxidation and hydrogen peroxide mechanisms which are represented as an inductive loop in EIS measurements of PEFCs has been developed in this study. The theoretical treatment was validated against EIS measurements carried out in an open-cathode stack and reported in the authors' previous study. The results show that the inductive loop in EIS measurements can only be accurately reproduced through the model that relates platinum oxide and hydrogen peroxide formation and not through a model that only accounts for either *PtO* or H_2O_2. The rate of platinum oxidation demonstrated to be the main mechanism that caused low performance in the open-cathode stack. Studies in the literature have focused on the role of platinum oxide on inductive loops of EIS measurements.

This study has demonstrated the importance of analysing EIS data through physics-based modelling for the correct interpretation of the electrochemical mechanisms that limit the performance of PEFCs. As different electrochemical mechanisms with different time constant and frequency dependence can be overlapped on the complex-pot. For instance, the model developed in this study predicted that oxygen transport mechanisms are overlapped with hydrogen peroxide mechanisms at low frequencies. This study has also demonstrated that multi-mechanisms that can cause low performance and degradation in PEFCs can be studied by combining modelling and EIS measurements in a complementary manner.

List of Symbols

b_i	inverse tafel slope, V^{-1}
Ca	double layer capacitance in anode, F/cm^2
c_i	concentration of chemical species *i* at the electrode surface, mol/cm^3
$c_{eq,i}$	concentration of chemical species *i* at equilibrium conditions, mol/cm^3
$c_O^{'}$	oxygen concentration at the CCL-PEM interface, mol/cm^3
D	effective diffusion coefficient, cm^2/sec
F	faraday constant, 96485 C/mol
j	imaginary component in impedance
$i_{Pt,f}$	forward current density A/cm^2
$i_{Pt,b}$	backward current density A/cm^2
$i_{0,i}$	exchange current density, A/cm^2
i_{ss}	steady-state current density, A/cm^2
$\tilde{i}$	deviation of variable i in the steady-state i_{ss}. A/cm^2
$k_{Pt,i}$	rate constant of platinum oxide formation reaction
P	parameter related to capacitance (constant phase element)
Ra	charge transfer resistance during HOR, $\Omega.cm^2$
R_i	charge transfer resistance, $\Omega.cm^2$

R_{ohm}	total ohmic resistance, PEM, GDL, Plate, $\Omega.cm^2$
R_W	resistance for the diffusion process, $\Omega.cm^2$
s	Laplace domain
T_W	time constant for the diffusion process, *sec*
t	time, sec
ω	angular frequency, *rad/sec*
Y	parameter related to capacitance, $(\sec)^P / \Omega.cm^2$
Za	impedance of anode, $\Omega.cm^2$
Zc	impedance of cathode, $\Omega.cm^2$
Z_{PEFC}	impedance of PEFC, $\Omega.cm^2$
Z_W	Warburg impedance, $\Omega.cm^2$
$Z^{'}$	real part of impedance
$Z^{''}$	imaginary part of impedance

Greek

β	maximum surface coverage by hydrogen peroxide, mol/cm^2
λ	maximum surface coverage by platinum oxide, mol/cm^2
$\gamma_{H_2O_2}$	fractional surface coverage of hydrogen peroxide, *dimensionless*
γ_{PtO}	fractional surface coverage of platinum oxide, *dimensionless*
γ_{eq,H_2O_2}	fractional surface coverage of hydrogen peroxide at equilibrium conditions, *dimensionless*
$\gamma_{eq,PtO}$	fractional surface coverage of platinum oxide at equilibrium conditions, *dimensionless*
$\gamma_{H_2O_2,ss}$	surface coverage of hydrogen peroxide at steady-state, *dimensionless*
$\gamma_{PtO,ss}$	surface coverage of platinum oxide at steady-state, *dimensionless*
$\tilde{\gamma}_{H_2O_2}$	deviation of variable $\gamma_{H_2O_2}$ in the steady-state $\gamma_{H_2O_2,ss}$, *dimensionless*
$\tilde{\gamma}_{PtO}$	deviation of variable γ_{PtO} in the steady-state $\gamma_{PtO,ss}$, *dimensionless*
δ	finite diffusion distance of oxygen transport from CCL-GDL to CCL-PEM interface, *cm*
η	overpotential in the CCL, *V*

$\tilde{\eta}$ deviation of variable η in the steady-state η_{ss}, *V*

η_{ss} steady-state overpotential, *V*

Figures

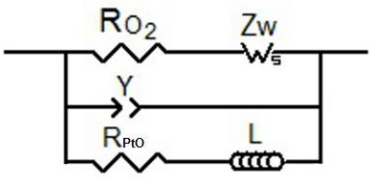

Figure 1. Electrical circuit representing electrochemical mechanisms in the ORR reaction with platinum oxidation

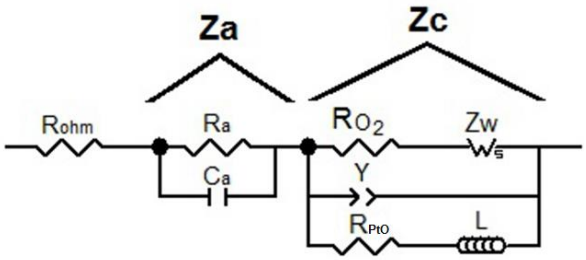

Figure 2. Electrical circuit representing the PEFC with PtO formation in Cathode

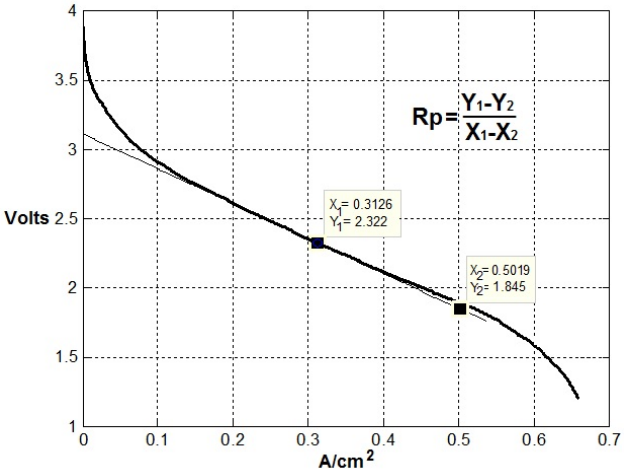

Figure 3. Polarisation curve and estimation of polarisation resistance *Rp* at 0.3125 A/cm^2.

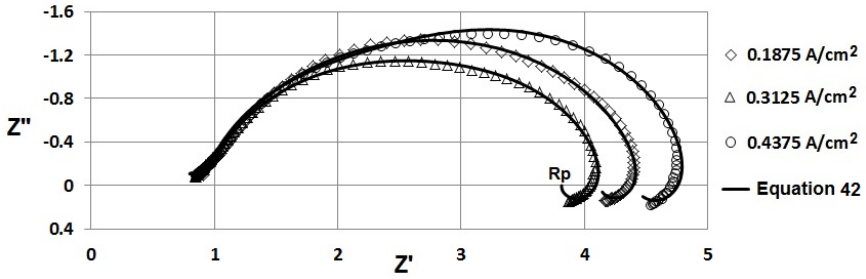

Figure 4. Comparison between experimental data and simulated data from Eq. 42

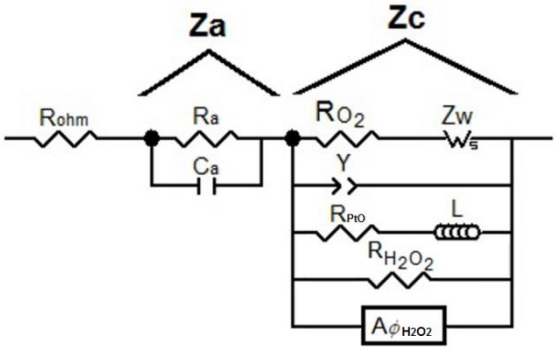

Figure 5. Electrical circuit representing the PEFC with PtO and H_2O_2 formation in Cathode

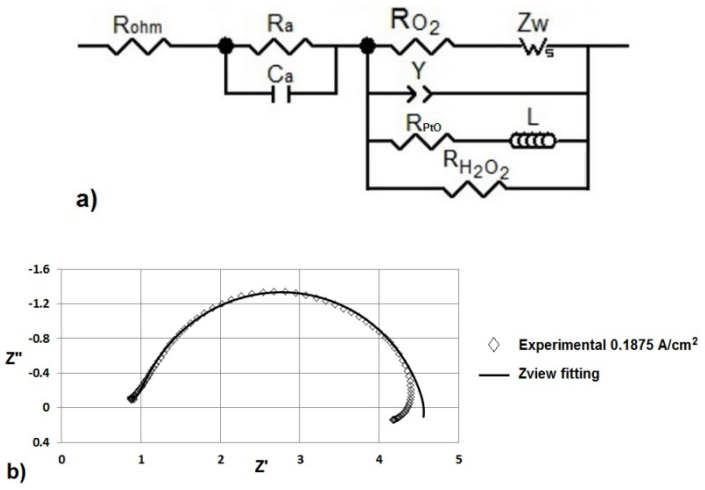

Figure 6. Zview analysis, a) circuit with no $A\phi_{H_2O_2}$ term, b) fitting result

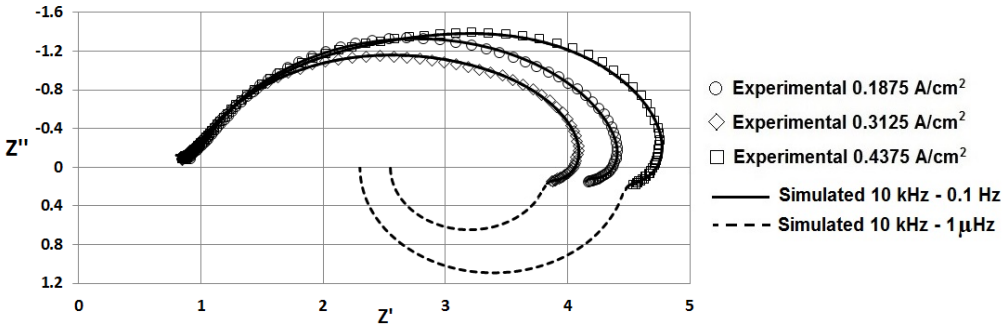

Figure 7. comparison between measured and simulated data using Eq. 65

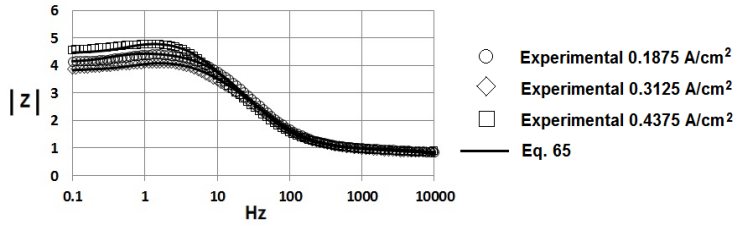

Figure 8. Comparison in Bode format (modulus) between measured and simulated data

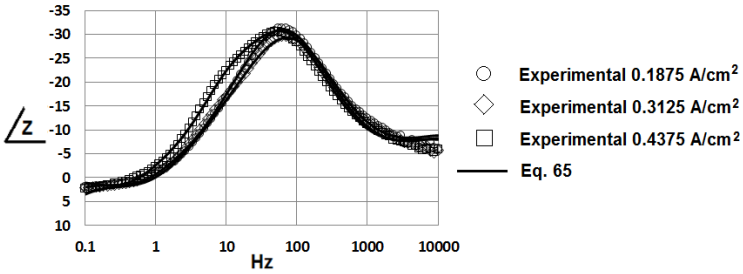

Figure 9. Comparison in Bode format (phase) between measured and simulated data

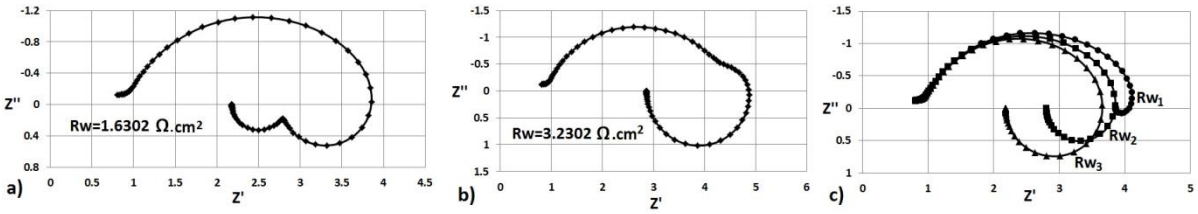

Figure 10. Effect of oxygen diffusion resistance on the impedance response considering Platinum oxidation mechanisms as negligible, a) reducing resistance, b) increasing resistance, c) reducing resistance from base case R_{W1}=2.6302 to R_{W2}=1.6302, and R_{W3}=0.6302 Ω.cm^2.

Tables

Current density A/cm^2	R_a Ω.cm^2	R_{O_2} Ω.cm^2	R_W Ω.cm^2	T_W sec	Y sec^P/Ω.cm^2	P dimensionless	τ_{PtO} sec	R_{PtO} Ω.cm^2
0.1875	0.2538	3.237	0.351	0.0142	0.00372	0.8307	0.4	28.9098
0.3125	0.2375	2.777	0.5224	0.037152	0.0047257	0.83071	0.5	23.45
0.4375	0.2375	2.3672	1.6121	0.0361	0.0038	0.8739	0.6	29.5

Table I Parameters of Eq. 42 extracted from measured data

Current density A/cm^2	R_a Ω.cm^2	R_{O_2} Ω.cm^2	R_W Ω.cm^2	T_W sec	Y sec^P/Ω. cm^2	P	$\tau_{H_2O_2}$ sec	$R_{H_2O_2}$ Ω.cm^2	R_{PtO} Ω.cm^2	τ_{PtO} sec
0.1875	0.2538	6.1213	0.5502	0.0249	0.0047	0.8158	0.2848	8.0328	6.0407	23.7
0.3125	0.2375	4.6459	2.6302	0.0458	0.0047	0.8028	0.2103	7.8285	3.7627	15.67
0.4375	0.2375	3.7787	3.7449	0.0405	0.0039	0.8408	0.2801	9.0656	2.1898	37.5

Table II Parameters of Eq. 65 extracted from measured data

References

[1] A. A. Topalov, S. Cherevko, A. R. Zeradjanin, J. C. Meier, I. Katsounaros and K. J. J. Mayrhofer, Chem. Sci., (2014), 5, 631-638.
[2] D. D. Macdonald, Electrochim. Acta, 51, (2006) pp. 1376-1388
[3] S. Cruz-Manzo and R. Chen, J. Electroanal. Chem., 694, (2013) pp. 45-55
[4] S. K. Roy, M.E. Orazem, B. Tribollet, J. Electrochem. Soc., 154, (2007) pp. B1378-B1388.
[5] M. Mathias, D. Baker, J. Zhang, Y. Liu, and W. Gu, , ECS Trans., 13 (13), (2008), pp. 129-152.
[6] B. P. Setzler and T. F. Fuller, J. Electrochem. Soc., 162, (2015) pp. F519-F530
[7] S. Cruz-Manzo, R. Chen, and P. Greenwood, J. Electroanal. Chem., 745, (2015) pp. 28-36
[8] S. Cruz-Manzo and R. Chen, J. Electrochem. Soc., 160, (2013) pp. F1109-F1115.
[9] S. K. Roy, H. Hagelin-Weaver, M. E. Orazem, J. Power Sources, 196, (2011), pp. 3736-3742.
[10] S. K. Roy and M. E. Orazem, ECS Trans., 3(1), 1031 (2006).
[11] H. Xu, R. Kunz, and J. M. Fenton, Electrochem. Solid-State Lett., 10, (2007), B1-B5.
[12] T. M. Arruda, B. Shyam, J. M. Ziegelbauer, S. Mukerjee, and D. E. Ramaker, J. Phys. Chem. C, 112, (2008), 18087.
[13] M. Teliska, W. E. O'Grady, and D. E. Ramaker, J. Phys. Chem. B, 109, (2005), 8076.
[14] Y. Liu, M. Mathias, and J. Zhang, Electrochem. Solid-State Lett., 13, (2010), B1-B3.
[15] A. P. Yadav, T. Okayasu, Y. Sugawara, A. Nishikata and T. Tsuru, *J. Electrochem. Soc*., 2012, 159, C190.
[16] R. M. Darling, and J. P. Meyers, J. Electrochem. Soc., 150, (2003), A1523-A1527.
[17] S. G. Rinaldo, J. Stumper, and M. Eikerling, J. Phys. Chem. C., (2010), 114, 5773-5785.
[18] J.-P. Diard, B. Le Gorrec and C. Montella, J. Electroanal. Chem., 326, 13 (1992).
[19] I. Epelboin, M. Keddam, and J. C. Lestrade, Faraday Discuss. Chem. Soc., 56, 264-275, (1973).
[20] Eikerling M., and Kornyshev A. A., J Electroanal. Chem., 475, (1999) pp. 107-123.
[21] D. Malevich, E. Halliop, B. A. Peppley, J. G. Pharoah, K. Karan, J. Electrochem. Soc. 156 (2009) B216-B224.
[22] N. Fouquet, C. Doulet, C. Nouillant, G. Dauphin-Tanguy, B. Ould-Bouamama, J. Power Sources 159 (2006) 920-928.
[23] C. H. Hsu and F. Mansfeld, *Corrosion* **57** (2001) 747-748.
[24] N. Wagner, J. Appl. Electrochem., 32, (2002), 859-863.
[25] Yuan X., Sun J. C., Blanco S., Wang H., Zhang J., and Wilkinson D. P., J. Power Sources, 161, (2006), pp. 929-937.

[26] Paganin V. A., Oliveira C. L. F., Ticianelli E. A., Springer T. E., and Gonzalez E. R., Electrochim. Acta, 43, (1998), 3761-3766.
[27] P.M Gomadam, and J. W. Weidner, Int. J. of Energy Res., 29, (2005), pp. 1133-1151.
[28] Q. Meyer, K. Ronaszegi, G. Pei-June, O. Curnick, S. Ashton, T. Reisch, P. Adcock, P. R. Shearing, D. J. L. Brett, J. Power Sources, 291, (2015) 261-269.
[29] R. Makharia, M. F. Mathias, and D. R. Baker, J. Electrochem. Soc., 152, (2005), pp. A970-A977
[30] M. Chandesris, C. Robin, M. Gerard, and Y. Bultel, Electrochim. Acta, 180, (2015), pp. 581-590.
[31] R. Antaño-Lopez, M. Keddam, and H. Takenouti, Electrochem. Soc. Proceedings 2000-24, pp. 11-22
[32] M. Keddam, O. R. Mottos, H. Takenouti, J. Electrochem. Soc., 128, (1981), pp. 257-266.
[33] S.Cruz-Manzo, R. Chen and P. Rama, Int. J. Hydrogen Energy, 38 (2013) 1702-1713